Effect of potassium on a model soot combustion: Raman and HRTEM evidences

L. Castoldi, R. Matarrese, L. Brambilla, A. Serafini, M. Tommasini & L. Lietti
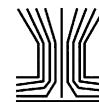
Effect of potassium on a model soot combustion: Raman and HRTEM evidences

L. Castoldi [ID][a], R. Matarrese [ID][a], L. Brambilla[b], A. Serafini[b], M. Tommasini[b], and L. Lietti[a]

[a]Dipartimento di Energia, Laboratory of Catalysis and Catalytic Processes and NEMAS, Centre of Excellence, Milano, Italy; [b]Dipartimento di Chimica, Materiali e Ingegneria Chimica "G. Natta," Politecnico di Milano, Milano, Italy

ABSTRACT

The effect of potassium on the oxidation of a model carbonaceous material (Printex U, namely, soot for brevity) has been investigated under isothermal conditions. For this purpose, Raman spectroscopy, Transmission Electron Microscopy (TEM), and Brunaure, Emmet, Teller surface area characterization have been applied to investigate structural changes occurring during soot oxidation both in the presence and in the absence of potassium. The Raman spectra of the model soot during combustion showed that oxidation preferentially involves the amorphous carbon fraction of the soot and only subsequently it affects the more ordered sp^2 domains. However, in the K-doped Printex U the oxidation of both the amorphous and more ordered sp^2 structures occurs concurrently. These findings have been confirmed by TEM analysis and explain the observed higher combustion activity of K-containing sample.

1. Introduction

Diesel engine emissions, particularly consisting of soot particles and NO_x, are source of environmental pollution and a concern for human health. Particulate matter from diesel exhausts consists of primary nano-metric soot particles that, after formation, coagulate to form micrometric chainlike aggregates, upon which heavy hydrocarbons, sulfates, nitrates, and water are adsorbed (Neeft et al. 1996a, b). Its physical size ($<$ 10 μm) is small enough to penetrate into the human lung and deposit in the pulmonary region where it may cause respiratory diseases.

The use of after-treatment devices to reduce NO_x and soot emissions generated by diesel engines is currently mandatory to meet European standards (Johnson 2008; Delphi website 2015). Diesel Particulate Filters (DPFs) are commonly used to remove soot particles from the exhausts *via* mechanical filtration; the combustion of trapped soot is then necessary in order to avoid pressure drops in the filter. This is a concern since the exhaust temperatures of diesel engines are too low to ensure the complete soot combustion (Darcy et al. 2007). For this purpose, "active regeneration" can be accomplished in the form of periodic thermal excursions to high tempera-tures by injecting a small amount of fuel upstream the DPF, whose combustion produces the required amount

of heat. However, in this case, an extra fuel consumption occurs; moreover, excessive heating can damage the filter and the other after-treatment devices.

Aiming at a low-temperature oxidation of the soot, the "passive regeneration" approach is also adopted. One possibility is to use NO_2, which is much more active than O_2 and therefore allows soot oxidation at lower temperature (above 250°C) (Cooper et al. 1990; Stan-more et al. 2001; Stanmore et al. 2008). In order to increase the concentration of NO_2, which is typically low (5%–15% of total NO_x), it is necessary to place a diesel oxidation catalyst upstream of the particulate filter. Such a process was used in the continuous regeneration trap (CRT) technology proposed by Johnson Matthey (Coo-per et al. 1990).

Moreover, in order to decrease the onset temperature for soot oxidation, a possibility is to create highly reactive soot, which makes it possible to regenerate diesel after-treatment systems at relatively low temperatures. It is well known that the presence of alkaline metals (and in lower extent of alkaline-earth metals) improves the soot oxidation, either alone or as promoters (Krishna and Makkee 2006; Aneggi et al. 2008). For example, in the carbon gasification with H_2O, CO_2, and O_2 (Gallagher and Harker 1964; McKee 1983; Moulijn et al. 1984; Hernández-Giménez et al. 2014), the activity of alkaline

CONTACT L. Castoldi ✉ lidia.castoldi@polimi.it 🖾 Dipartimento di Energia, Laboratory of Catalysis and Catalytic Processes and NEMAS, Centre of Excellence, via La Masa 34 - 20156 Milano, Italy.

metals decreased along the sequence Cs, K, Na, Li, and the same order was found in the diesel soot oxidation (Neeft et al. 1996a, b). However, the thermal stability is one of the main drawbacks of alkaline metals-containing soot combustion catalysts. Pt-K/Al$_2$O$_3$ was investigated and it was found that platinum and potassium exhibited synergetic effects in soot combustion activity (Krishna and Makkee 2006; Matarrese et al. 2007; Pieta et al. 2010), but their stability is still not satisfactory (Krishna and Makkee 2006). The degradation of potassium catalysts due to the sublimation of potassium compounds during the soot combustion process was also reported (Mul et al. 1995; An and McGinn 2006; López-Suárez et al. 2009). For this reason, the use of specific supports able to stabilize potassium has been proposed (Jiménez et al. 2006; Ogura et al. 2008; Zhang et al. 2010) in order to overcome the problem related to the alkaline loss.

The reaction mechanism in the C oxidation in the presence of alkalis is not completely clarified. It has been suggested that the C combustion passes through the formation of some different oxygenated intermediate species (Kapteijn et al. 1984; Zhu et al. 2000) favored by the presence of alkali metals and/or that the alkali are directly involved in the process thanks to the formation of low melting point compounds, thus improving the mobility of the active surface species and favoring the contact between the soot and the catalyst, which represents a key factor in the oxidation of soot (Neeft et al. 1996a, b; Querini et al. 1999; An and McGinn 2006).

Along these lines, the reactivity of soot greatly increases by direct impregnation of soot with alkaline (Na, K, Cs) or alkaline/earth (Ca, Ba, Mg) metals (Castoldi et al. 2009). Under these "full contact" conditions, it was found that the reactivity in the soot combustion is considerably improved and nicely correlates with the electronic properties (i.e., electronegativity) of the investigated metal ions.

Within this scenario, the aim of this work is to investigate more in details the role of alkali metals in the oxidation of soot. In particular, the focus is to investigate whether the presence of potassium (taken as representative alkaline metal) may affect the molecular structure of soot during the oxidation process, giving an explanation of the low oxidation temperature of soot in the presence of alkali.

Since the composition of real diesel particulate is affected by several engine operation characteristics such as load, speed, and operating temperatures, as the amount of SOF (soluble organic fraction) highly depends on cylinder temperature (Fino et al. 2003), it is difficult to collect batches of soot with constant properties. For this reason, the present study has been performed by using an amorphous synthetic carbon (Printex U by

Degussa) whose properties have been well assessed in the literature (e.g., in Nejar et al. 2007; Atribak et al. 2010; Wang-Hansen et al. 2011) and which is typically used as model soot (see the review by Stanmore et al. 2008). This material was chosen to avoid any interference due to the presence of adsorbed HCs, sulfates, or fly ash present in real diesel soot. Moreover, Printex U is more difficult to burn than real diesel soot (Nejar et al. 2007), making the results conservative (Fino et al. 2006), particularly for catalyzed soot combustions investigations (Hernández-Giménez et al. 2014).

Printex U and K-doped Printex U samples (indicated as model soot and K-soot for brevity) have been oxidized for different time lengths under isothermal conditions and then carefully characterized. Three different techniques have been used to characterize the soot and K-soot samples at different oxidation degree: (i) X-ray diffraction (XRD) analysis that permits to calculate the crystallites size and the distance between carbon layers (i.e., it gives structural information) but unfortunately these parameters are an average over a volume of about 1 mm^3; (ii) high-resolution Transmission Electron Microscopy (HRTEM) that permits to directly obtain images of carbon layers and their arrangement in space, i.e., soot nanostructure; and (iii) Raman spectroscopy, which is commonly used to characterize carbonaceous materials at the molecular level, principally using the I_D/I_G ratio as indication of the sp^2/sp^3 relative concentration (Tunistra and Koenig 1970; Castiglioni et al. 2004; Ferrari 2007; Le Guillou et al. 2007; Vázquez-Santos et al. 2012; Pawlyta et al. 2015). Due to its peculiar sensitivity on the sp^2/sp^3 structure of carbonaceous materials, Raman spectroscopy has been successfully used in the literature to characterize both real diesel soot and model compounds. For instance, several authors have characterized with Raman spectroscopy the relative amounts of graphite-like structures and amorphous carbon in soot particles and have studied their modification under different uncatalyzed and catalyzed oxidation conditions (Sadeszky et al. 2005; Al-Qurashi and Boehman 2008; Knauer et al. 2009a, b; Atribak et al. 2010; López-Suárez et al. 2011; Luperta et al. 2012; Gaddam et al. 2016).

2. Experimental

2.1. Materials

Printex U (Evonik Degussa, Essen, Germany) was used as model soot (hereafter referred to as soot). The full contact sample has been prepared by direct impregnation of soot with aqueous solution of the K nitrate salt (in the following indicated as K-soot). The selected metal

loading was 1.06 mmol/g_{soot}. After impregnation, the K-soot sample has been dried at 100°C in air for 2 h.

The specific surface area (SA, m^2/g) was determined for both fresh and oxidized model soot and K-soot by N_2 adsorption/desorption at −196°C with the Brunaure, Emmet, Teller (BET) method using a Micromeritics TriStar 3000.

Oxidation experiments have been performed in a flow-reactor equipment consisting of a quartz tube reactor (7 mm I.D.) connected to a mass spectrometer (Thermostar 200, Pfeiffer Vacuum) and to a micro GC (Agilent 3000A) for the online analysis of the gases exiting the reactor. In each test, 80 mg of K-doped sample or pure soot have been used. Before each test, the samples were heated at 500°C in He. The oxidation of both soot and K-soot samples has been carried out under isothermal conditions at 200°C in He + 5% v/v O_2 + 500 ppm NO_2 + 2% v/v H_2O or at 450°C in He + 5% v/v O_2 + 2% v/v H_2O up to the desired soot conversion. The gas analysis performed by MS (mass spectrometer) and GC (gas chromatograph) online instruments allows to carefully quantify both CO_2 and CO produced during the soot oxidation. The % soot conversion χ has been calculated using the following Equation (1):

$$\chi(\%) = \frac{mol(CO_2 + CO)}{mol(C_{soot})} * 100 \qquad [1]$$

where mol(CO_2+CO) are the moles of CO_x formed during the soot oxidation runs and mol(C_{soot}) are the moles of C in the Printex U calculated assuming that the model soot is constituted by carbon (molecular weight = 12).

2.2. X-ray diffraction

X-ray diffraction measurements were performed on both fresh Printex U and K-doped Printex U samples using a Philips PW 1050/70 X-ray powder diffractometer with graphite filtered copper radiation (Cu K_α: $\lambda = 1.542$ Å). The diffraction patterns were recorded at room temperature in the 2θ range from 10 to 70θ (resolution 0.05θ). The distance between carbon layers (d_{002}) has been evaluated according to the Bragg Equation (2):

$$d_{002} = \frac{\lambda}{2sin\theta_{002}} \qquad [2]$$

where the X-ray wavelength is $\lambda = 1.542$ Å and θ_{002} is the position of the (002) band in the XRD spectrum.

The layer thickness in our samples has been evaluated by calculating the L_c parameter according to the Debye–Scherrer formula (3):

$$L_c = \frac{0.89\lambda}{\beta_{002}cos\theta_{002}} \qquad [3]$$

L_c and d_{002} parameters thus calculated (Pawlyta et al. 2015) will be compared with those estimated by HRTEM analysis (see below).

2.3. TEM measurements

TEM was performed on Printex U and K-doped Printex U samples, both fresh and oxidized, using a Philips CM200 electron microscope operating at 200 kV equipped with a Field Emission Gun filament (resolution in the lattice fringe mode 0.14 nm). Soot samples were dispersed in methanol by ultrasonic agitation and dropped onto a 200 mesh lacey carbon-coated copper grid. A Gatan US 1000 CCD camera was used and 2048 × 2048 pixels images with 256 gray levels were recorded. Soot and K-soot were characterized by coupling two imaging mode: low magnification bright field to image the soot nanoparticles, and high-resolution TEM to image the structural organization of the carbon layers inside the soot nanoparticles. During acquisition of TEM and HRTEM images, the samples did not undergo structural transformation. Care is taken to work with low beam current densities and short acquisition times. Particle primary size was determined by measuring the diameter of the soot particles and fitting the measured statistical distributions, obtained with more than 500 counts, with a log-normal function. To evaluate the HRTEM micrographs, a fringe analysis with the software ImageJ has been performed. In order the basic steps are: (1) image selection and application of a minimum filter; (2) thresholding to isolate the lattice fringes; (3) erode and removal of dark outliers; (4) skeletonization (an example is reported in Figure 1). These steps allowed to obtain binary images with one-pixel width lines that can be used for extracting the parameters of the Basic Structure Unit (BSU) like the stacking layer length L_a, the layer thickness L_c, and the interlayer spacing between carbon layers d_{002} (Palotas et al. 1996; Müller et al. 2007; Alfe et al. 2009). An illustration of L_a, L_c, and d_{002} is showed in the lattice fringe image reported in Figure 1d.

2.4. Raman spectroscopy

The Raman spectra of Printex U and K-doped Printex U samples at different oxidation degrees have been recorded with a Horiba Labram HR800 Raman spectrometer coupled to an Olympus BX41 microscope (50 X objective) and a 50 mW Melles Griot HeNe laser at
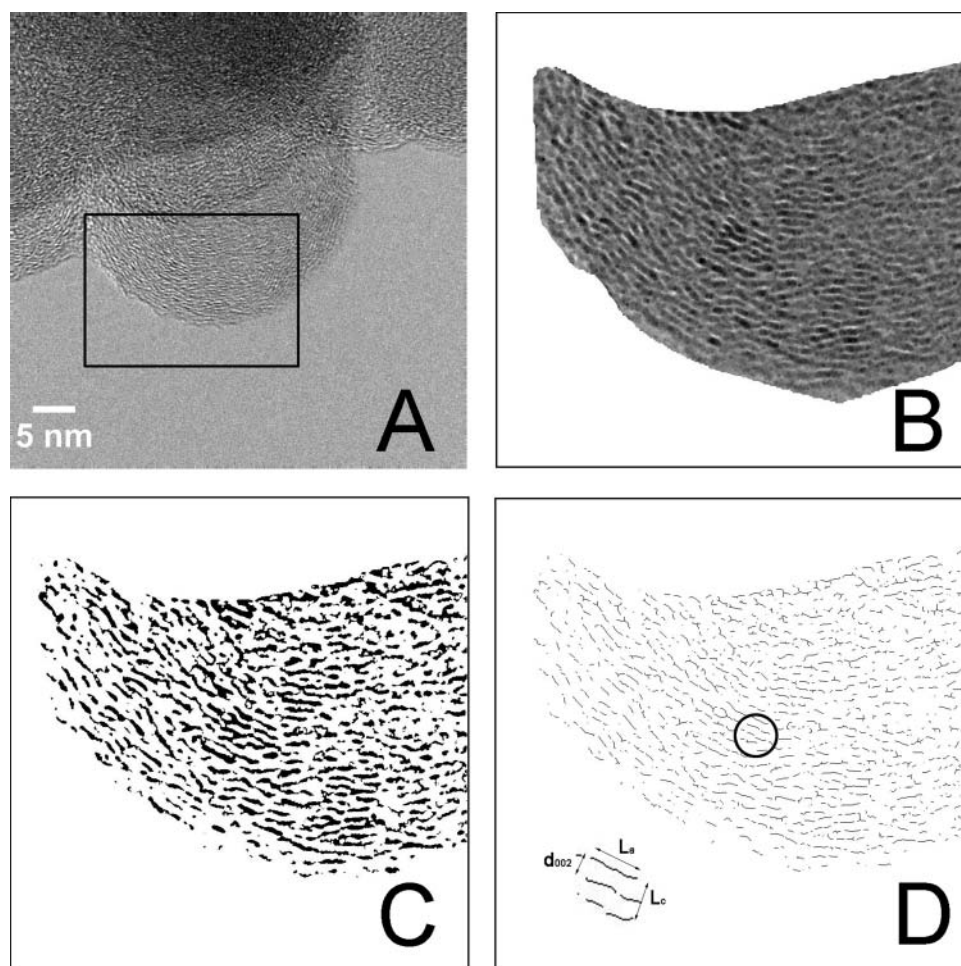
Figure 1. Fringes extraction from Printex U HRTEM micrograph: (A) image selection; (B) filtered image; (C) threshold analysis; (D) skeletonized image (in the inset is shown the BSU parameters evaluated in the fringe analysis).

632.8 nm. All spectra were collected in the 700–2100 cm^{-1} spectral range with a laser power on the sample of 500 μW. The spectra were obtained as average of four acquisitions each one lasting for 50 s. Samples were prepared depositing a small amount of soot or K-soot powder on a glass slide and then gently pressed with a spatula in order to obtain a compact and homogenous surface. We have verified that the parameters used (*i.e.*,

laser power, laser wavelength, acquisition time, and compact samples surface) assured a good reproducibility of the spectra with no undesired extra effects. In fact, excessive laser power induces two effects: (i) a reversible red-shift of the position of the Raman peaks due to heating (Ferrari and Basko 2013) and (ii) an irreversible change of the band shape over the G and D region. The process (ii) can be taken as an indication of undesired laser-induced modification of the sample microstructure.

3. Results and discussion

3.1. *Characterization of starting materials*

The specific surface area of soot and K-soot samples (both fresh and oxidized) has been investigated by BET analysis, which reveals a value close to 90 m^2/g for fresh soot. A slightly lower value has been determined for K-soot (see Table 1).

Unoxidized soot and K-soot have been analyzed by X-ray diffraction (see Figure 2). As it clearly appears from

Table 1. BET analysis (SA, m^2/g) at different soot conversion values.

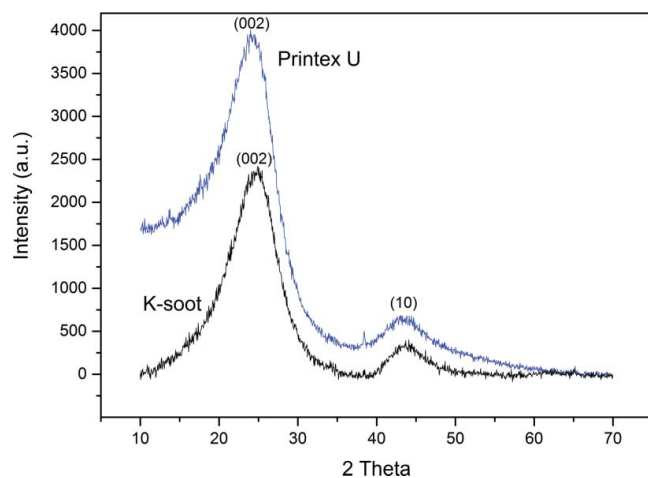| Soot conversion (%)	SA (m^2/g)	
	Soot	K-soot
Fresh	90	75
8	153	—
11	219	81
20	246	185
40	367	286
50	330	—
60	270	—
64	—	580

Figure 2. XRD measurement of unoxidized soot and K-soot samples.

the figure, no reflexes of K-containing species are recognizable in the K-soot. However, since the K-soot sample has been dried at 100°C, it is likely that K is present in the form of dispersed nitrate species. On the other hand, two broad lines of carbon are well recognized in the XRD diffraction spectra, the (002), and (10) reflections. In Table 2, the average distance between carbon layers (d_{002}) and the L_c parameter are reported. As it appears, for both soot and K-soot, similar d_{002} (0.368 nm and 0.359 nm, respectively) and L_c (1.11 nm and 1.15 nm, respectively) values have been found which are also consistent with those reported in the literature (Pawlyta et al. 2015). Accordingly, it is possible to appreciate that the addition of potassium does not modify mainly the amorphous structure of soot.

Figure 3 shows the bright field TEM observations made before heat-treatment for soot (a, b) and K-soot (c, d) samples. In both cases, the presence of micrometer-sized aggregates (see Figures 3a and c) of much smaller spherical particles is visible; the mean diameter of the elemental particles was found to be 20 nm for the soot and 21 nm for the K-soot (see Table 2) in agreement with several literature indications (Nejar et al. 2007; Wang-Hansen et al. 2011; Liu et al. 2010).

Furthermore, both Figures 3b and d clearly show the alignment of graphitic platelets. The largest primary particles are nearly spherical and show a concentric nanostructure; this organization seems to develop to the same extent in the absence and in the presence of potassium, suggesting that the addition of K does not modify the main morphological features of soot material. This appearance is confirmed by the HRTEM fringe analysis that exhibits similar L_c, L_a, and d_{002} in the unoxidized soot and K-soot; these structural parameters are also in good agreement with the values obtained in XRD (see Table 2).

A typical example of the first-order region of the Raman spectra in the case of unoxidized soot and K-soot samples is presented in Figure 4. For the K-soot samples, we do not observe any signal at 1054 cm^{-1}, which is the characteristic strongest Raman line of KNO_3 (Liu et al. 1992). This is consistent with XRD results. Raman spectra show two main peaks located at about 1340 cm^{-1} and 1590 cm^{-1}. These two broad and overlapping signals are characteristic of carbon black and other related carbonaceous materials with similar structure, such as soot. These Raman signals are assigned to the G ("graphite") peak at 1590 cm^{-1} and to the D ("defect") peak at 1340 cm^{-1}. Due to resonance effects, the D peak position depends on the laser excitation line used for the experiments (Castiglioni et al. 2004; Ferrari 2007; Le Guillou et al. 2007; Nejar et al. 2007; Ivleva et al. 2007; Knauer et al. 2009a, b; Vázquez-Santos et al. 2012; Pawlyta et al. 2015). In graphite samples, the G peak is associated with in-plane nuclear displacements affecting the CC bond stretching coordinates; the nuclear displacement pattern correlates with the ring-stretching Raman mode of benzene observed close to 1600 cm^{-1}.

The D peak, which is known to be a characteristic feature of disordered graphite, is associated with a collective totally symmetric ring-breathing mode. Its relative intensity with respect to the G peak (I_D/I_G) increases with the increasing degree of disorder in the graphitic structure (Nejar et al. 2007; Knauer et al. 2009a, b). It is evident from Figure 4 that the Raman spectra of unoxidized soot and K-soot are practically superimposable, showing that
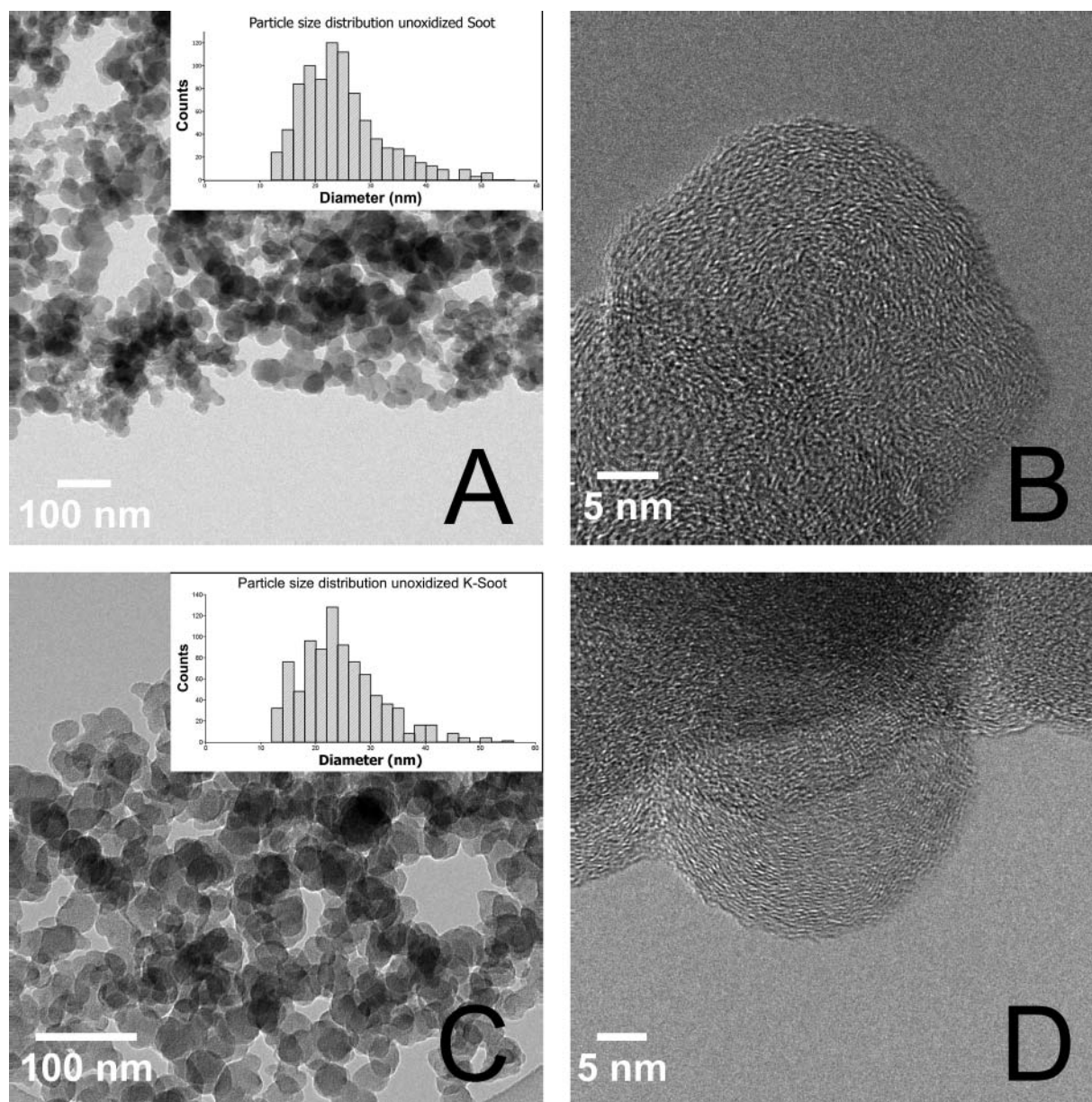
Table 2. Primary size distributions obtained by TEM measurements, XRD, and TEM crystallographic parameters (the mean interlayer spacing between carbon layers d_{002} (nm), average height L_c (nm), and average width L_a (nm) of BSU) of soot and K-soot samples at different oxidation degrees.

Sample	Mean diameter (nm)	σ^- (nm)	$\sigma+$ (nm)	d_{002}(nm) From XRD	d_{002}(nm) From TEM	L_c (nm) From XRD	L_c (nm) From TEM	L_a (nm) From TEM
Soot	22	7	11	0.368	0.379	1.11	1.02	0.78
K-soot	21	8	12	0.359	0.377	1.15	0.98	0.81
Oxidized soot—60%	20	9	15		0.371		1.25	1.18
Oxidized K-soot—64%	19	9	16		0.376		1.05	0.78

Figure 3. TEM images of fresh samples. (A) Low magnification bright field TEM micrograph of fresh Printex U; (B) High resolution TEM of fresh Printex U; (C) Low magnification bright field TEM micrograph of fresh K-doped Printex U; (D) High resolution TEM of fresh K-doped Printex U. The insets in A and C report the primary particle size distributions of fresh Printex U and K-doped Printex U, respectively.

at molecular level the overall structure of the soot sample is unaffected by the presence of potassium.

In conclusion, based on BET, XRD, TEM, and Raman spectroscopy findings, there is no evidence of structural changes introduced by the presence of potassium in our fresh soot-containing samples.

3.2. Soot oxidation under isothermal conditions

The oxidation of soot has been carried out under isothermal conditions for both soot and K-soot samples, flowing O_2 (5% v/v) in He at 450°C or O_2 (5% v/v) + NO_2 (500 ppm) in He at 200°C up to the desired soot conversion, evaluated according to Equation (1). In all experiments, 2% (v/v) of H_2O is present. Note that prior to soot oxidation, the samples have been heated at 500°C in He. This leads to nitrate decomposition in the K-doped Printex U samples; accordingly, it is expected that K is present as carbonate and nitrate species in the runs carried out with O_2 and O_2 + NO_2, respectively. This is in line with the easy carbonation of the K species and the displacement of carbonates by nitrates in case of NO_x-containing feed (Castoldi et al. 2010a, b).

In Figure 5, the Raman spectra of soot (Figure 5a) and K-soot (Figure 5b) samples oxidized up to 40% in either O_2 or NO_2+O_2 atmosphere are reported. As it clearly
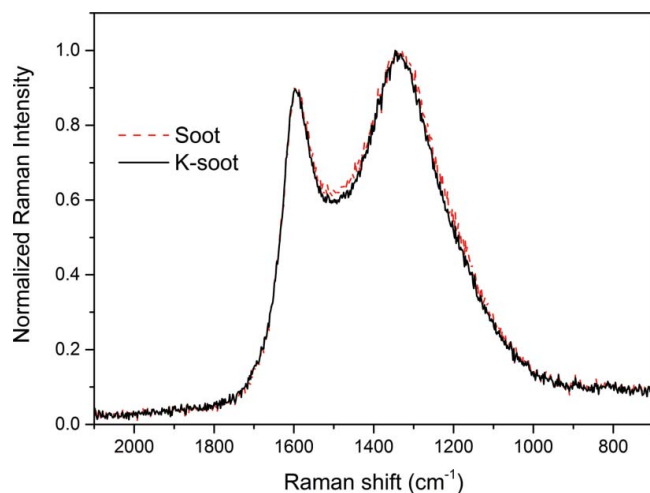
Figure 4. Raman spectra (632 nm excitation, 100 μW laser power) recorded over fresh Printex U and K-doped Printex U samples.

appears, all spectra show D and G signatures; moreover, there are no marked differences in the Raman spectra as a function of the oxidizing species. Accordingly, the presence of NO_2 in the gas phase seems not affecting the morphological/structural-features of samples, whereas it has a remarkable effect on the rate of the oxidation process (data here not reported).

In Figure 6, the Raman spectra of soot samples at different oxidation degrees (curve a = 0%, b = 20%, c = 40%, d = 50%, e = 60%) under isothermal conditions at 200°C in O_2/NO_2 mixture are reported. As oxidation proceeds, we observe changes of the broad Raman signal placed between the D and the G peak: this broad component, associated with amorphous sp^3 carbon structures (Sadezky et al. 2005), decreases, while the D and the G lines sharpen. This observation suggests that oxidation preferentially begins on the amorphous carbon fraction of the soot and only subsequently it may involve the more ordered sp^2 domains.

TEM analysis of the oxidized soot sample at low oxidation degree (not reported) closely resembles those in Figure 3, where it is possible to recognize the graphitic platelets within soot nanoparticles. It is possible to conclude that at low oxidation stage the more ordered sp^2 structure of soot is preserved since oxidation preferentially affects the amorphous part. In Figure 7, the TEM images of partially oxidized soot (oxidation degree near 60%) are reported; in particular the low magnification bright field TEM micrograph is reported in Figure 7a and high-resolution TEM in Figure 7b. The inset in Figures 7a and b shows the primary particle size distribution and the fringes extracted images of the areas indicated by the boxes, respectively. As it appears, mean diameter, size distribution, and main morphology
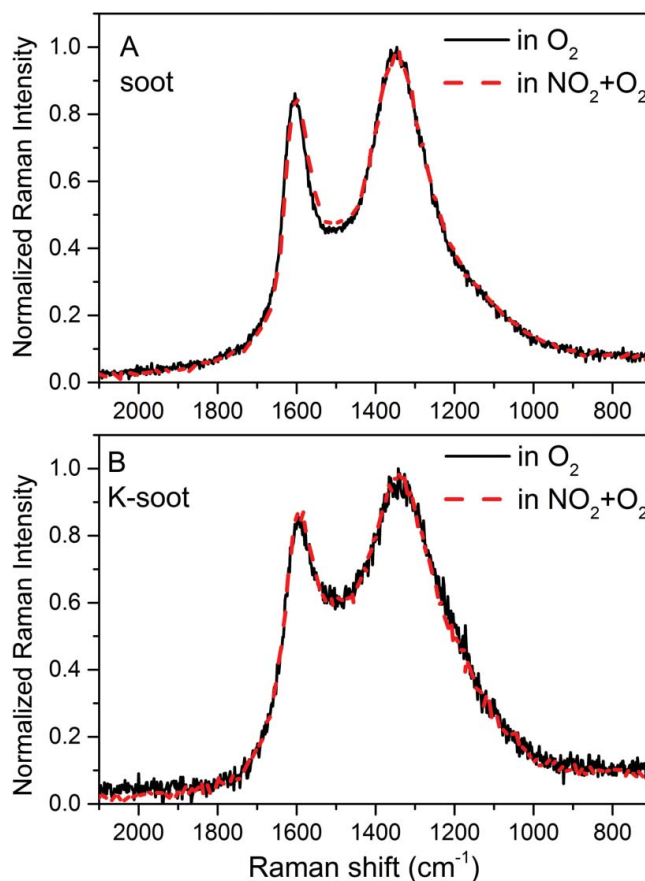

Figure 5. Raman spectra (632 nm excitation, 100 μW laser power) recorded over oxidized Printex U (A) and K-doped Printex U (B) samples under O_2 and O_2/NO_2 (oxidation state near 40% in both cases).

features of the highly oxidized soot are similar to the unoxidized samples of soot and K-soot (see Table 2). On the other hand, the fringes analysis of HRTEM images reveals that higher values of L_a and L_c are achieved for
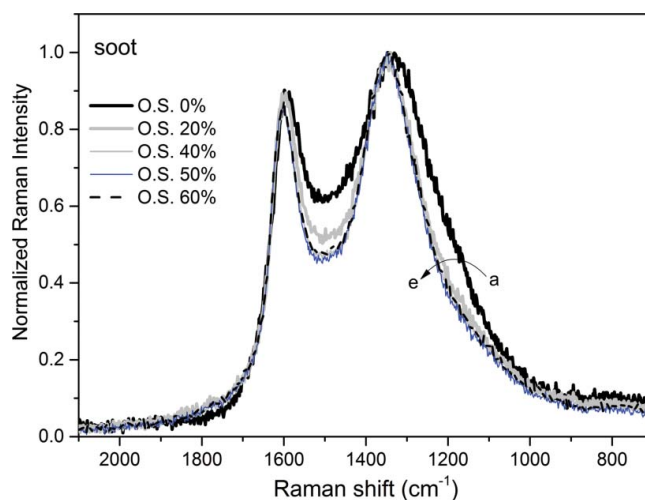

Figure 6. First-order Raman spectra of Printex U at different oxidation degrees (curve a = 0%, b = 20%, c = 40%, d = 50%, e = 60 %) under O_2/NO_2 at 200°C.
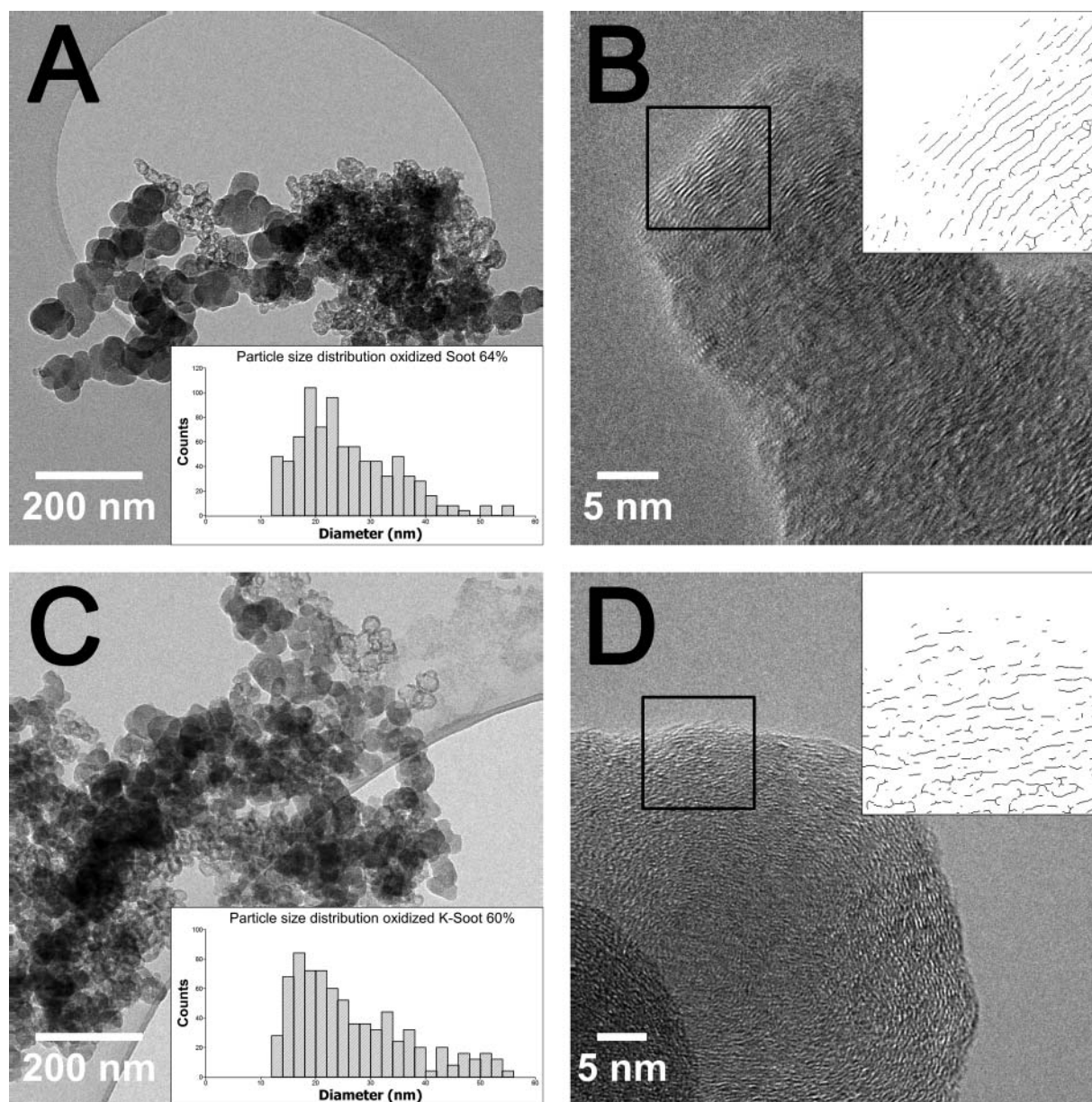
Figure 7. TEM images of partially oxidized samples (60% in the case of Printex U, 64% in the case of K-doped Printex U). (A) Low magnification bright field TEM micrograph of oxidized Printex U; (B) High resolution TEM of oxidized Printex U; (C) Low magnification bright field TEM micrograph of oxidized K-doped Printex U; (D) High resolution TEM of oxidized K-doped Printex U. Insets in B and D report the fringes extracted images of the areas indicated by the boxes. The area in the inset B (oxidized Printex U 60%) clearly exhibits a higher graphitization degree (higher La and Lc) in comparison to the inset D (oxidized K-doped Printex U 64%). The insets in A and C report the primary particle size distributions of oxidized Printex U 60% and K-doped Printex U 64%, respectively.

the 60% oxidized soot compared to the unoxidized soot and K-soot (see Table 2). From these results, it is evident that a structural improvement occurs in the soot at high degree of oxidation.

The faster oxidation of the amorphous component with respect to the graphitic is likely associated with an increase in roughness and porosity of soot, with a consequent increase of the specific surface area (see the values reported in Table 1). This is in fact observed during the

Printex U oxidation process until 40% of soot conversion. Afterward, the surface area tends to slightly decrease. As reported by Stanmore et al. (2001), generally there is an increase in the surface area during the oxidation process, with values rising up to 50% burnout. For higher soot conversion values, the surface area may remain roughly constant, or decrease. The change in area depends on the gasification medium and the temperature and many other factors. More recent studies

(Yezerets et al. 2005; Strzelec et al. 2013) have clearly shown that the extent of the area increase depends on the nature of the soot samples, implying that there are significant differences in their individual burning modes. In our case, the surface area tends to decrease at high soot conversion values possibly due to the fact that the oxidation of the less amorphous part does not lead to the development of a significant surface roughness.

In Figure 8, the Raman spectra of oxidized K-soot sample at different oxidation degrees (curve $a = 0\%$, $b = 10\%$, $c = 15\%$, $d = 20\%$, $e = 40\%$, $f = 64\%$) under O_2/NO_2 at 200°C are reported. At variance to the case of soot, the Raman spectra of K-soot seems to be unaffected by oxidation; D and G peaks and the signal from amorphous sp^3 carbon structures preserve their shapes and relative intensities (i.e., all the Raman signals are almost superimposed, as it appears in Figure 8 and in the insert). This suggests that potassium promotes the oxidation of both the amorphous sp^3 and more ordered sp^2 structures at the same time. The constant shape of Raman spectra of K-soot with oxidation is indicative of a rather stable packing of graphitic planes and platelet size distribution as oxidation proceeds, i.e., the relative amount of organized sp^2 structures vs. amorphous sp^3 is rather constant.

TEM images of highly oxidized K-soot (oxidation degree near 64%) are reported in Figure 7; in particular the low magnification bright field TEM micrograph are reported in Figure 7c and high-resolution TEM in Figure 7d. The inset in Figures 7c and d reports the primary particle size distribution and the fringes extracted images of the areas indicated by the boxes, respectively.
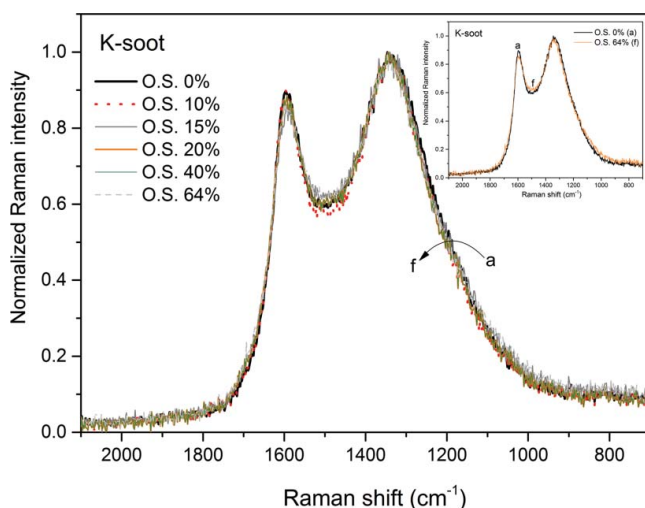

Figure 8. First-order Raman spectra of K-doped Printex U at different oxidation degrees (curve a = 0%, b = 10%, c = 15%, d = 20 %, e = 40 %, f = 64 %) under O_2/NO_2 at 200°C.

As opposed to un-doped soot, K-soot exhibits no significant variations of the structural parameters at high degree of oxidation. Indeed, similar values of morphological and structural data extrapolated from TEM micrographs for the unoxidized and 64% oxidized K-soot are obtained (see Table 2). It is worth to note that comparing the area in the inset B (oxidized soot 60%) with that of inset D (oxidized K-soot 64%), a higher graphitization degree (higher L_a and L_c) is clearly apparent.

From the data reported above, it is clear that the alkaline oxide, i.e., potassium, is involved in some of the oxidation steps of soot.

It is well known in the literature (Stanmore et al. 2001; Setiabudi et al. 2004) that the non-catalytic soot oxidation occurs via the involvement of chemisorbed oxygen (either coming from O_2 or NO_2), which reacts with carbon sites; the formation of chemisorbed oxygen species leads to CO and CO_2 production as primary products. Note that under non-catalytic condition, the CO/CO_2 ratio is dependent on the supply of oxygen and on the temperature.

From the morphological point of view, the heat-treatment of soot causes a partial structural changes (i.e., the so-called "graphitization degree" increases), resulting in a lower G band-width, as already described from spectra reported in Figure 6. Such graphitization is visible also from the fringe analysis of the HRTEM images, where the presence of coherent domains gives higher value of L_c and L_a parameters (see Table 2).

When alkaline metals are present, such as K or others, the chemisorption of oxygen is favored with formation of different oxygenated species, as already discussed in the literature (Radovic et al. 1983; Moulijn et al. 1984; Aneggi et al. 2008; Castoldi et al. 2009). The specific role of alkaline seems to be favoring the oxygen transfer from the gas phase to the carbon surface, thanks to their electron-donating effect that increases the local electron density of neighboring C-C sites promoting their affinity for binding an oxygen atom (Chen and Yang 1997). Accordingly, this results in a weakening of the C-C bonds, thus favoring the carbon gasification process.

In the case of K-soot sample, the Raman spectra in Figure 8 have shown that D and G bands keep their width unchanged and also the intensity ration of the two bands is almost constant, suggesting that in K-soot both the sp^2 and sp^3 carbon fractions are efficiently removed. Accordingly, in this case the presence of K seems to inhibit the structural change. Also the fringe analysis of the HRTEM images confirms this statement; indeed, the structural parameters L_c, L_a achieved for the oxidized K-soot closely resemble the values obtained for the soot and K-soot unoxidized samples.

4. Conclusions

In this study, the effect of potassium on the oxidation of a model soot (Printex U) has been investigated. For this purpose, K-soot samples have been prepared by deposition of potassium on the model soot; both the model soot and the K-soot samples have been oxidized under isothermal conditions and analyzed by Raman spectroscopy at different degrees of carbon conversion. Raman and TEM analysis revealed a clear correlation between the structure of soot undergoing combustion and its reactivity. In particular, on the bare model soot material, the Raman spectra showed that the oxidation involves initially the amorphous part, and then the crystalline fraction. Soot combustion is enhanced in the presence of potassium: in fact the Raman spectra of K-soot samples showed that potassium promotes the oxidation of both the amorphous and the crystalline structures. The observed effect of potassium in accelerating soot oxidation can be related to the weakening of the C-C bonds in both the amorphous sp^3 and more ordered sp^2 carbon structures, and this promotes the carbon gasification process. This provides a rationale for the promoting effect of potassium on the oxidation of carbonaceous materials.

Based on these observations, the presence of alkalis can be exploited in practical application in diesel particulate traps to enhance the soot oxidation, provided that a proper contact is guaranteed between K and soot.

ORCID

L. Castoldi   http://orcid.org/0000-0002-7962-1146
R. Matarrese   http://orcid.org/0000-0002-3499-6614

References

Alfè, M., Apicella, B., Barbella, R., Rouzaud, J.-N., Tregrossi, A., and Ciajolo, A. (2009). Structure-Property Relationship in Nanostructures of Young and Mature Soot in Premixed Flames. *Proc. Combust. Inst.*, 32:697–704.

Al-Qurashi, K., and Boehman, A. L. (2008). Impact of Exhaust Gas Recirculation (EGR) on the Oxidative Reactivity of Diesel Engine Soot. *Combust. Flame*, 155:675–695.

An, H. M., and McGinn, P. J. (2006). Catalytic Behavior of Potassium Containing Compounds for Diesel Soot Combustion. *Appl. Catal. B: Environ.*, 62:46–56.

Aneggi, E., de Leitenburg, C., Dolcetti, G., and Trovarelli, A. (2008). Diesel Soot Combustion Activity of Ceria Promoted with Alkali Metals. *Catal. Today*, 136:3–10.

Atribak, I., Bueno-López, A., and García-García, A. (2010). Uncatalysed and Catalysed Soot Combustion under $NO_x + O_2$: Real Diesel versus Model Soots. *Combust. Flame*, 157:2086–2094.

Castiglioni, C., Tommasini, M., and Zerbi, G. (2004). Raman Spectroscopy of Polyconjugated Molecules and Materials: Confinement Effect in One and Two Dimensions. *Philos. T. Roy Soc. A*, 362:2425–2459.

Castoldi, L., Lietti, L., Nova, I., Matarrese, R., Forzatti, P., Vindigni, F., Morandi, S., Prinetto, F., and Ghiotti, G. (2010a). Alkaline- and Alkaline-Earth Oxides based Lean NO_x Traps: Effect of the Storage Component on the Catalytic Reactivity. *Chem. Eng. J.*, 161:416–423.

Castoldi, L., Lietti, L., Forzatti, P., Morandi, S., Ghiotti, G., and Vindigni, F. (2010b). The NO_x Storage-reduction on Pt-K/Al_2O_3 Lean NO_x Trap Catalyst. *J. Catal.*, 276:335–350.

Castoldi, L., Matarrese, R., Lietti, L., and Forzatti, P. (2009). Intrinsic Reactivity of Alkaline and Alkaline-earth Metal Oxide Catalysts for Oxidation of Soot. *Appl. Catal. B: Environ.*, 90:278–285.

Chen, S. G., and Yang, R. T. (1997). Unified Mechanism of Alkali and Alkaline Earth Catalyzed Gasification Reactions of Carbon by CO_2 and H_2O. *Energy Fuels*, 11:421–427.

Cooper, J., Jyung, H. J., and Thoss, J. E. (1990). Treatment of Diesel Exhaust Gases. US Patent 4,902,487.

Darcy, P., Da Costa, P., Mellottée, H., Trichard, J.-M., and Djéga-Mariadassou, G. (2007). Kinetics of Catalyzed and Non-catalyzed Oxidation of Soot from a Diesel Engine. *Catal. Today*, 119:252–256.

Delphi website (2015). Worldwide Emissions Standards 2015-2016. Available at http://delphi.com/manufacturers/auto/powertrain/emissions_standards/

Ferrari, A. C. (2007). Raman Spectroscopy of Graphene and Graphite: Disorder, Electron-Phonon Coupling, Doping and Nonadiabatic Effects. *Solid State Commun.*, 143:47–57.

Ferrari, A. C., and Basko, D. M. (2013). Raman Spectroscopy as Versatile Tool for Studying the Properties of Graphene. *Nature Nanotechnol.*, 8:235–246.

Fino, D., Russo, N., Badini, C., Saracco, G., and Specchia, V. (2003). Effect of Active Species Mobility on Soot-Combustion over Cs-V Catalysts. *AiChE J.*, 49:2173–2180.

Fino, D., Russo, N., Saracco, G., and Specchia, V. (2006). Catalytic Removal of NO_x and Diesel Soot Over Nanostructured Spinel-type Oxides. *J. Catal.*, 242:38–47.

Gaddam, C. K., Vander Wal, R. L., Chen, X., Yezerets, A., and Kamasamudram, K. (2016). Reconciliation of Carbon Oxidation Rates and Activation Energies based on Changing Nanostructure. *Carbon*, 98:545–556.

Gallagher, J. T., and Harker, H. (1964). Reaction of Carbon with Oxidizing Gases: Catalysis by Compounds of Iron, Cobalt and Nickel. *Carbon*, 2:163–173.

Hernández-Giménez, A. M., Lozano Castelló, D., and Bueno-López, A. (2014). Diesel Soot Combustion Catalysts: Review of Active Phases. *Chem. Papers*, 68:1154–1168.

Ivleva, N. P., Messerer, A., Yang, X., Niessner, R., and Pöschl, U. (2007). Raman Microspectroscopic Analysis of Changes in the Chemical Structure and Reactivity of Soot in a Diesel Exhaust Aftertreatment Model System. *Environ. Sci. Technol.*, 41:3702–3707.

Jiménez, R., García, X., Cellier, C., Ruiz, P., and Gordon, A..L. (2006). Soot Combustion with K/MgO as Catalyst. *Appl. Catal. A: Gen.*, 297:125–134.

Johnson, T. (2008). Diesel Engine Emissions and Their Control. *Platinum Metals Rev.*, 52(1):23–37.

Kapteijn, F., Abbel, G., and Moulijn, J. A. (1984). CO_2 Gasification of Carbon Catalysed by Alkali Metals. *Fuel*, 63:1036–1042.

Knauer, M., Carrara, M., Rothe, D., Niessner, R., and Ivleva, N. P. (2009a). Changes in Structure and Reactivity of Soot

During Oxidation and Gasification by Oxygen, Studied by Micro-Raman Spectroscopy and Temperature Programmed Oxidation. *Aerosol Sci. Technol.*, 43:1–8.

Knauer, M., Schuster, M. E., Su, D., Schlögl, R., Niessner, R., and Ivleva, N. P. (2009b). Soot Structure and Reactivity Analysis by Raman Microspectroscopy, Temperature-Programmed Oxidation, and High-Resolution Transmission Electron Microscopy. *J. Phys. Chem. A*, 113:13871–13880.

Krishna, K., and Makkee, M. (2006). Soot Oxidation over NO_x Storage Catalysts: Activity and Deactivation. *Catal. Today*, 114:48–56.

Lapuerta, M., Oliva, F., Agudelo, J. L., and Boehman, A. L. (2012). Effect of Fuel on the Soot Nanostructure and Consequences on Loading and Regeneration of Diesel Particulate Filters. *Combust. Flame*, 159:844–853.

Le Guillou, C., Brunet, F., Irifune, T., Ohfuji, H., and Rouzaud, J.-N. (2007). Nanodiamond Nucleation Below 2273 K at 15 GPa from Carbons with Different Structural Organizations. *Carbon*, 45:636–648.

Liu, D., Ullman, F. G., and Hardy, J. R. (1992). Raman Scattering and Lattice-dynamical Calculations of Crystalline KNO_3. *Phys. Rev. B*, 45:2142–2147.

Liu, J., Zhao, Z., Xu, C., Duan, A., and Jiang, G. (2010). Comparative Study on Physicochemical Properties and Combustion Behaviors of Diesel Particulates and Model Soot. *Energy Fuels*, 24:3778–3783.

López-Suárez, F. E., Bueno-López, A., Illán-Gómez, M. J., Ura, B., and Trawczynski, J. (2009). Potassium Stability in Soot Combustion Perovskite Catalysts. *Top. Catal.* 52:2097–2100.

López-Suárez, F. E., Bueno-López, A., Illán-Gómez, M. J., Ura, B., and Trawczynski, J. (2011). Study of the Uncatalyzed and Catalyzed Combustion of Diesel and Biodiesel Soot. *Catalysis Today*, 176:182–186.

Matarrese, R., Castoldi, L., Lietti, L., and Forzatti, P. (2007). High Performances of Pt-K/Al_2O_3 Versus Pt-Ba/Al_2O_3 LNT Catalysts in the Simultaneous Removal of NO_x and Soot. *Top. Catal.*, 42/43:293–297.

McKee, D. W. (1983). Mechanisms of the Alkali Metal Catalysed Gasification of Carbon. *Fuel*, 62:170–175.

Moulijn, J. A., Cerfontain, M. B., and Kapteijn, F. (1984). Mechanism of the Potassium CO_2 Catalysed Gasification of Carbon in CO_2. *Fuel*, 63:1043–1047.

Mul, G., Neeft, J. P. A., Kapteijn, F., Makkee, M., and Moulijn, J. A. (1995). Soot Oxidation Catalyzed by a Cu/K/Mo/Cl Catalyst: Evaluation of the Chemistry and Performance of the Catalysts. *Appl. Catal. B: Environ.*, 6:339–352.

Müller, J.-O., Su, D. S., Wild, U., and Schlögl, R. (2007). Bulk and Surface Structural Investigations of Diesel Engine Soot and Carbon Black. *Phys. Chem. Chem. Phys.*, 9:4018–4025.

Neeft, J. P. A., Makkee, M., and Moulijn, J. A. (1996a). Diesel Particulate Emission Control. *Fuel Process. Technol.*, 47:1–69.

Neeft, J. P. A., Makkee, M., and Moulijn, J. A. (1996b). Catalysts for the Oxidation of Sootfrom Diesel Exhaust Gases. I. An Exploratory Study. *Appl. Catal. B: Environ.*, 8:57–78.

Nejar, N., Makkee, M., and Illán-Gómez, N. J. (2007). Catalytic Removal of NOx and Soot from Diesel Exhaust: Oxidation Behaviour of Carbon Materials used as Model Soot. *Appl. Catal. B: Environ.*, 75:11–16.

Ogura, M., Morozumi, K., Elangovan, S. P., Tanada, H., Ando, H., and Okubo, T. (2008). Potassium-doped Sodalite: A Tectoaluminosilicate for the Catalytic Material Towards Continuous Combustion of Carbonaceous Matters. *Appl. Catal. B: Environ.*, 77:294–299.

Palotas, A. B., Rainey, L. C., Feldermann, C. J., Sarofim, A. F., and Sande, J. B. V. (1996). Soot Morphology: An Application of Image Analysis in High-resolution Transmission Electron Microscopy. *Microsc. Res. Technol.*, 33:266–278.

Pawlyta, M., Rouzaud, J.-N., and Duber, S. (2015). Raman Microspectroscopy Characterization of Carbon Blacks: Spectral Analysis and Structural Information. *Carbon*, 84:479–490.

Pieta, I. S., García-Diéguez, M., Herrera, C., Larrubia, M. A., and Alemany, L. J. (2010). In situ DRIFT–TRM Study of Simultaneous NO_x and Soot Removal over Pt–Ba and Pt–K NSR Catalysts. *J. Catal.*, 270:256–267.

Querini, C. A., Cornaglia, L. M., Ulla, M. A., and Miró, E. E. (1999). Catalytic Combustion of Diesel Soot on Co,K/MgO Catalysts. Effect of the Potassium Loading on Activity and Stability. *Appl. Catal. B: Environ.*, 20:165–177.

Radovic, L. R., Walker Jr., P. L., and Jenkins, R. G. (1983). Importance of Catalyst Dispersion in the Gasification of Lignite Chars. *J. Catal.*, 82:382–394.

Sadezky, A., Muckenhuber, H., Grothe, H., Niessner, R., and Poeschl, U. (2005). Raman Microspectroscopy of Soot and Related Carbonaceous Materials. *Carbon*, 43:1731–1742.

Setiabudi, A., Makkee, M., and Moulijn, J. A. (2004). The Role of NO_2 and O_2 in the Accelerated Combustion of Soot in Diesel Exhaust Gases. *Appl. Catal. B: Environ.*, 50:185–194.

Stanmore, B., Brilhac, J. F., and Gilot, P. (2001). The Oxidation of Soot: A Review of Experiments, Mechanisms and Models. *Carbon*, 39:2247–2268.

Stanmore, B., Tschamber, V., and Brilhac, J. F. (2008). Oxidation of Carbon by NOx, with Particular Reference to NO_2 and N_2O. *Fuel*, 87:131–146.

Strzelec, A., Toops, T. J., and Daw, C. S. (2013). Oxygen Reactivity of Devolatilized Diesel Engine Particulates from Conventional and Biodiesel Fuels. *Energy Fuels*, 27:3944–3951.

Tunistra, F., and Koenig, J. L. (1970). Raman Spectrum of Graphite. *J. Chem. Phys.*, 53:1126–1130.

Vázquez-Santos, B. M., Geissler, E., László, K., Rouzaud, J-N., Martínez-Alonso, A., and Tascón, J. M. D. (2012). Comparative XRD, Raman, and TEM Study on Graphitization of PBO-Derived Carbon Fibers. *J. Phys. Chem. C*, 116:257–268.

Wang-Hansen, C., Kamp, C. J., Skoglundh, M., Andersson, B., and Carlsson, P. A. (2011). Experimental Method for Kinetic Studies of Gas Solid Reactions: Oxidation of Carbonaceous Matter. *J. Phys. Chem. C* 115:16098–16108.

Yezerets, A., Currier, N. W., Kim, D. H., Eadler, H. A., Epling, W. S., and Peden, C. H. F. (2005). Differential Kinetic Analysis of Diesel Particulate Matter (Soot) Oxidation by Oxygen Using a Step–response Technique. *Appl. Catal. B: Environ.*, 61:120–129.

Zhang, Z., Zhang, Y., Wang, Z., and Gao, X. (2010). Catalytic Performance and Mechanism of Potassium-supported Mg–Al Hydrotalcite Mixed Oxides for Soot Combustion with O_2. *J. Catal.*, 271:12–21.

Zhu, Z. H., Lu, G. Q., and Yang, R. T. (2000). New Insights into Alkali-Catalyzed Gasification Reactions of Carbon: Comparison of N_2O Reduction with Carbon over Na and K Catalysts. *J. Catal.*, 192:77–87.